Title

Copper nanoparticle ensembles for selective electroreduction of CO_2 to C_2-C_3 products.

Journal

Proceedings of the National Academy of Sciences of the United States of America, 114(40)

ISSN

0027-8424

Authors

Kim, Dohyung
Kley, Christopher S
Li, Yifan
et al.

Publication Date

2017-10-01

DOI

10.1073/pnas.1711493114

Peer reviewed

Copper nanoparticle ensembles for selective electroreduction of CO_2 to C_2–C_3 products

Dohyung Kim[a,b,c], Christopher S. Kley[d], Yifan Li[b,c,d], and Peidong Yang[a,b,c,d,1]

[a]Department of Materials Science and Engineering, University of California, Berkeley, CA 94720; [b]Chemical Sciences Division, Lawrence Berkeley National Laboratory, Berkeley, CA 94720; [c]Kavli Energy NanoScience Institute, Berkeley, CA 94720; and [d]Department of Chemistry, University of California, Berkeley, CA 94720

Contributed by Peidong Yang, August 15, 2017 (sent for review June 27, 2017; reviewed by Matthew Kanan and Kyung Byung Yoon)

Direct conversion of carbon dioxide to multicarbon products remains as a grand challenge in electrochemical CO_2 reduction. Various forms of oxidized copper have been demonstrated as electrocatalysts that still require large overpotentials. Here, we show that an ensemble of Cu nanoparticles (NPs) enables selective formation of C_2–C_3 products at low overpotentials. Densely packed Cu NP ensembles underwent structural transformation during electrolysis into electrocatalytically active cube-like particles intermixed with smaller nanoparticles. Ethylene, ethanol, and *n*-propanol are the major C_2–C_3 products with onset potential at −0.53 V (vs. reversible hydrogen electrode, RHE) and C_2–C_3 faradaic efficiency (FE) reaching 50% at only −0.75 V. Thus, the catalyst exhibits selective generation of C_2–C_3 hydrocarbons and oxygenates at considerably lowered overpotentials in neutral pH aqueous media. In addition, this approach suggests new opportunities in realizing multicarbon product formation from CO_2, where the majority of efforts has been to use oxidized copper-based materials. Robust catalytic performance is demonstrated by 10 h of stable operation with C_2–C_3 current density 10 mA/cm^2 (at −0.75 V), rendering it attractive for solar-to-fuel applications. Tafel analysis suggests reductive CO coupling as a rate determining step for C_2 products, while *n*-propanol (C_3) production seems to have a discrete pathway.

heterogeneous catalysis | electrocatalysis | CO_2 reduction | copper nanoparticles | in situ structural transformation

With rising concerns about the anthropogenic impacts of current trends in energy use, as well as the prospect of continuing these trends to meet future needs (1), we are at a stage where revolutionary change to our energy paradigm is a must. Various methods for effectively using solar energy are being developed to power and support the global population (2–4). Among them, artificial photosynthesis is considered vital to meeting our goal toward long-term global sustainability (5). The successful introduction of artificial photosynthesis technology will highly depend on the development of every functional component essential to the efficient operation of the overall system.

As energy from sunlight eventually ends up in chemical bonds by the photocatalytic or electrocatalytic component, development of an effective catalytic material to facilitate the conversion process becomes important. Over the past several decades, the focus has been on using water as the starting substrate and converting it to hydrogen gas (6). More recently, carbon dioxide has been considered as a promising substrate, and many efforts have been underway to find efficient electrocatalysts that can selectively operate for reducing CO_2 in aqueous solutions against the competing hydrogen evolution (7–16). However, major progress has been limited to two-electron reduced products of CO and formate. Still, the formation of multicarbon products involving multiple proton and electron transfers remains as one of the biggest scientific challenges to be addressed.

Starting from the idea that element copper is a key component to forming multicarbon products (17, 18), there have been various studies so far where formation of products such as C_2H_4, C_2H_6, and C_2H_5OH has been observed often with the requirement of large overpotentials (potential applied ≤−1 V vs. RHE) (19–35). These methods mostly rely on reducing certain forms of oxidized copper (19–25, 27–30, 32–34) (either oxides or halides) and even this approach has been extended to reduce carbon monoxide instead (36), a common intermediate for CO_2 reduction, to circumvent difficulties associated with C–C coupling starting from CO_2. Furthermore, to instead create a favorable environment for multicarbon product formation, there have been attempts to use gas-diffusion electrodes with alkaline electrolytes (37). It would certainly be desirable to discover an electrocatalyst that can directly reduce CO_2 to multicarbon products with high selectivity and energy efficiency (i.e., minimal energy loss from low overpotentials).

Here, we show that an ensemble of densely packed copper nanoparticles (NPs) could enable selective conversion of CO_2 to multicarbon products, while significantly suppressing C_1 formation. Catalytically active cube-like structures, capable of forming ethylene, ethanol, and *n*-propanol, are formed during electrolysis by the structural transformation of the Cu NP ensemble. These structures can selectively generate C_2 and C_3 products together at low overpotentials in neutral pH aqueous media, illustrating the importance of in situ structural evolution in CO_2 electrocatalysis. We also find that the catalyst support plays an important role for high multicarbon selectivity. This work suggests an alternative route to development of catalysts for multicarbon products and understanding of their formation, where the field has been heavily reliant on using oxidized copper as starting materials.

Significance

Electrochemical conversion of CO_2 to carbon-based products, which can be used directly as fuels or indirectly as fuel precursors, is suggested as one of the promising solutions for sustainability. Not only does this process allow using renewables such as solar electricity as energy input, but CO_2 emitted from the consumption process can be recycled back into fuels. The success of this technology depends on the value added to the product that forms from CO_2, and therefore it is important to facilitate multicarbon product generation. This work presents a copper-based catalyst, formed in situ from an ensemble of nanoparticles, that is able to selectively generate C_2–C_3 products at low overpotentials with good stability, where their efficient formation has been difficult to achieve.

Author contributions: D.K. and P.Y. designed research; D.K., C.S.K., and Y.L. performed research; D.K., C.S.K., and Y.L. analyzed data; and D.K. and P.Y. wrote the paper.

Reviewers: M.K., Stanford University; and K.B.Y., Sogang University.

Conflict of interest statement: Provisional patent application filed based on the technology described in this work.

[1]To whom correspondence should be addressed. Email: p_yang@berkeley.edu.

This article contains supporting information online at www.pnas.org/lookup/suppl/doi:10.1073/pnas.1711493114/-/DCSupplemental.

Results and Discussion

Monodisperse Cu NPs (size 6.7 nm) prepared (*SI Appendix*, Fig. S1) were directly deposited onto carbon paper support (1 cm^2_{geo}) to form densely packed NP ensembles. Cu NP loading was systematically increased (*SI Appendix*, Table S1) starting from the lowest loading of ~2 μg of Cu (×1). Number density of NPs was determined based on the estimated surface area of the carbon paper support (24, 26) (*SI Appendix*, Fig. S2), which was at ~5.9 cm^2_{real}/cm^2_{geo} (roughness factor ~5.9). Most of the NPs are isolated at the lowest loading condition, and increased loadings resulted in densely packed arrangements of Cu NPs (Fig. 1*A*). In the case of ×22.5 loading, the surface was mostly covered with closely packed Cu NPs (*SI Appendix*, Fig. S3).

Cu NP ensembles with varied loading densities were tested for their electrocatalytic CO_2 reduction activity, under identical conditions of 0.1 M $KHCO_3$ at 1 atm CO_2. From product analysis (*SI Appendix*, Fig. S4), we found that increased loadings resulted in a drastic rise of the C_2–C_3 faradaic efficiency (FE) (Fig. 1*B* and *SI Appendix*, Fig. S5 and Table S2). This trend is consistent with the observed loss of C_1 products, indicating that carbon-based intermediates could be effectively coupled to yield

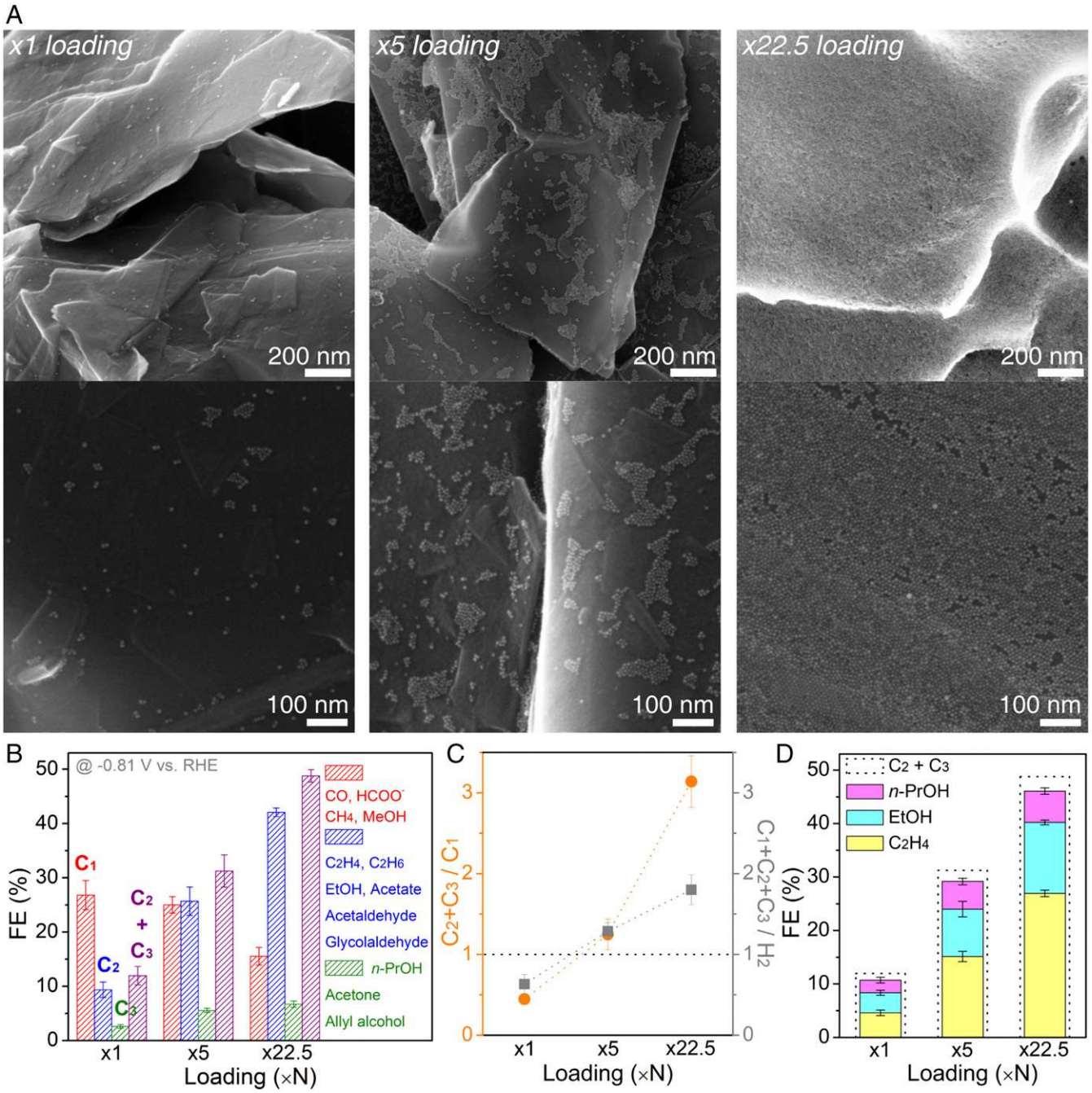

Fig. 1. Varied density of Cu NP ensembles and their electrocatalytic activity. (*A*) SEM images of Cu NPs loaded on carbon-paper support at ×1 loading, ×5 loading, and ×22.5 loading. (*B*) FEs (%) for C_1, C_2, and C_3 products. (*C*) Relative ratio of the FEs. (*D*) Ethylene, ethanol, and *n*-propanol FE with the dotted line showing the overall C_2–C_3 FE. Activity measured at −0.81 V vs. RHE, using 0.1 M $KHCO_3$ saturated under 1 atm CO_2. Error bars shown in *B*–*D* are 1 SD from three independent measurements.

multicarbon products. When plotting the relative ratio of the C_2–C_3 FE to C_1 FE (Fig. 1*C*), charge consumed to reduce CO_2 was mainly from the reaction pathways to C_2–C_3 products at increased loading conditions, reaching up to 76% out of the total CO_2 reduction products. Similar trends can be seen with CO_2 reduction dominating over the competing H_2 evolution (Fig. 1*C*). Among various C_2–C_3 products, ethylene (C_2H_4), ethanol (EtOH), and *n*-propanol (*n*-PrOH) were the majority, constituting 94% out of the total C_2–C_3 products generated (Fig. 1*D*).

When probing the product distribution over time for the ×22.5 loading condition, an abrupt change occurred during the initial period (Fig. 2*B*). Hydrogen was the dominant product when gas products were measured 3 min after the start of electrolysis. Selectivity for C_2H_4 increased afterward. A similar trend was found for the liquid products as well (*SI Appendix*, Fig. S6), where liquids analyzed for the first 7 min had less multicarbon products relative to formate. Visual inspection of the electrode (*SI Appendix*, Fig. S7) also supported the fact that product distribution was shifting during its initial electrochemical testing, as more gas bubbles were observed at the beginning of electrolysis, probably due to the majority of charge being consumed for two-electron transfer products, such as hydrogen.

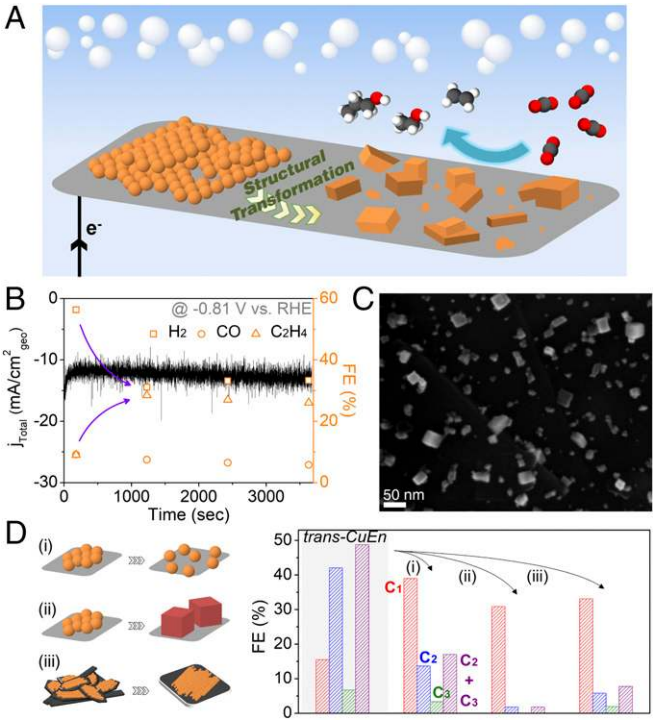

Fig. 2. Structural transformation of Cu NP ensembles. (*A*) Schematic illustrating the transformation process of Cu NP ensembles to an active catalyst for C_2–C_3 product formation. (*B*) Total current density (based on geometric area) versus time plot for ×22.5 loading condition at −0.81 V vs. RHE. FE of gas products are shown at the time point of measurement. FE of CH_4 and C_2H_6 are omitted because of their low values. (*C*) SEM image of ×22.5 loaded carbon-paper support electrode after 7 min of electrolysis at −0.81 V vs. RHE. (*D*) Investigation of the parameters affecting structural transformation of Cu NP ensembles and their catalytic activity. Three different conditions have been tested: (*i*) separation of the NPs from their initial densely packed assembly, (*ii*) use of Cu nanocubes as starting materials, and (*iii*) change of support to a low surface area carbon plate. FE of C_1, C_2, and C_3 products obtained from trans-CuEn (left column, shaded, at −0.81 V vs. RHE) are compared with the activity measured for three different conditions [at (*i*) −0.84 V, (*ii*) −0.86 V, and (*iii*) −0.81 V vs. RHE, respectively]. Electrochemical tests were conducted using 0.1 M $KHCO_3$ solution at 1 atm CO_2.

This observation indicated that the NP ensemble may go through a structural transformation process during initial electrolysis. Instead of the starting densely packed Cu NPs (×22.5 loading, Fig. 1*A*), cube-like particles (10 ∼ 40 nm) mixed together with smaller NPs were observed on the carbon support after electrolysis (*SI Appendix*, Fig. S8). Carbon-paper supports with lower loading were also checked after electrolysis and a trend could be observed: the more densely packed the Cu NPs, the more likely the formation of cube-like particles (*SI Appendix*, Fig. S9). When Cu NPs were sparsely covering the support, random aggregates of NPs together with the pristine NPs could be found after electrolysis. Surface-area analysis of Cu NP ensembles after electrolysis also showed that the densely packed NPs transformed to larger particles (*SI Appendix*, Fig. S10). As expected, loss of surface ligands during electrolysis and structural transformation was confirmed by elemental analysis (*SI Appendix*, Figs. S11 and S12). Structural transformation of the NP ensemble (Fig. 2*A*) occurred during the initial stage of electrolysis. This was confirmed from observation of the electrode 7 min after the start of electrolysis (Fig. 2*C*), which coincided with the shift in catalytic activity (Fig. 2*B*). Negligible catalytic activity of the underlying carbon paper (*SI Appendix*, Fig. S13) further supports that the structure derived from Cu NP ensembles is responsible for enhanced C_2–C_3 formation. This catalytically active structure formed starting from densely packed Cu NP ensembles (×22.5 loading on carbon-paper support in 0.1 M $KHCO_3$), hereafter referred to as trans-CuEn, was further investigated.

As the initial loading density of Cu NP ensembles (and their densely "packed-ness") tends to govern their structural transformation during electrolysis and resulting electrochemical activity, we tried to intentionally separate the Cu NPs in the precursor state to trans-CuEn. We expected the transformation process to cube-like structures to be disrupted, leading to diminished C_2–C_3 selectivity. Cu NPs (×22.5 loading) were mixed with carbon black before depositing on carbon-paper support (*SI Appendix*, Fig. S14), which led to NPs being spatially separated from each other. Under this condition, substantial loss of C_2–C_3 product selectivity (FE from 49 to 17%) was observed (Fig. 2*D*), while CO and $HCOO^-$ became major products. When particles were examined after electrolysis, the structure more resembled what would be observed for low-density conditions (*SI Appendix*, Figs. S9 and S14). Cu NPs have been observed to electrically fuse into irregularly shaped large crystals under strong bias conditions (<−1.25 V vs. RHE), reaching a similar state irrespective of the initial conditions (38). Here, we find that structural transformation can be caused not only under low bias conditions, but controlled by the initial arrangement of NPs, and consequently catalytic behavior for multicarbon products can be significantly improved.

As trans-CuEn displays cubic-shaped particles, copper nanocubes loaded onto carbon-paper support were tested under identical conditions for comparison. We used Cu nanocubes that have been previously studied for CO_2 reduction (26) (*SI Appendix*, Fig. S15). Specifically, cubes with edge length 25 nm were used (with copper loading mass identical to trans-CuEn) to approximately match the cubic-shaped particles that vary in size (10 ∼ 40 nm) for trans-CuEn. In contrast to trans-CuEn, observed structural changes were minimal where the cubes seem to have sintered or roughened (*SI Appendix*, Fig. S16). Furthermore, only small amounts of multicarbon products were detected (Fig. 2*D*). The result is consistent with the earlier report of Cu nanocubes, which claims multicarbon product formation at high overpotentials (<−1 V vs. RHE) (26). Therefore, we find that simple reproduction of the key morphological feature present in trans-CuEn is insufficient to reach high multicarbon selectivity.

This leads to the possibility of cube-like particles derived in situ during electrolysis featuring unique active sites for C_2–C_3 formation. Recently, scanning tunneling microscopy

investigation of copper for carbon monoxide reduction has shown not only the reconstruction of a polycrystalline surface to a (100) surface, but also the additional structural transformation unique to the (100) reconstructed copper, leading to stepped surfaces which selectively generate ethanol (39, 40). While this observation may have been for reducing CO, together with the findings here, it brings into attention the importance of in situ structural transformation for multicarbon product formation in copper-based catalysts. In addition, we would like to point out that while the vast majority of research has been to use oxide-derived structures, with even some reports claiming the importance of remaining oxidized copper (29, 41), the catalytically active structure derived here is from pristine Cu NPs (with a thin layer of surface oxide naturally present). Furthermore, we find that the structural transformation observed is unique to the original Cu NPs (*SI Appendix*, Fig. S17). Therefore, it would be important to understand how this structural transformation proceeds and what type of active site motifs are present under working conditions. This is especially the case for copper, which may oxidize after electrolysis, possibly leading to the loss of surface atomic information (*SI Appendix*, Fig. S12). However, we also cannot rule out the possibility that high multicarbon selectivity stems from having a mixture of particles (42), which are the cube-like ones together with smaller particles. With all of these taken into consideration, further investigation into the structural origin of high multicarbon selectivity from Cu NP ensembles is needed.

Furthermore, we investigated the role of the catalyst support by depositing Cu NPs onto a highly polished graphite plate (1 cm^2_{real}, roughness factor ~1), while keeping the NP density (/cm^2_{real}) identical to that of trans-CuEn. Structural transformation occurred in a similar way resulting in cubic-shaped particles (*SI Appendix*, Fig. S18). However, H_2 and C_1 products were the major products (Fig. 2*D* and *SI Appendix*, Fig. S18). We speculate that this difference is due to local pH effects discussed in earlier reports (32, 43–46), as the loss in the real surface area of the underlying support led to a sharp decrease of the geometric current density (lowered to ≈1/5 of the original). The increased local pH by large current density of trans-CuEn (on carbon-paper support) could play a role in determining its catalytic behavior. Therefore, it seems that it is important to not only start from a high density of closely packed Cu NPs to facilitate the structural transformation, but also have the underlying support provide sufficient surface area. This shows why high C_2–C_3 selectivity was not observed from the previous report of Cu NP monolayers (16).

Catalytic activity of trans-CuEn was further probed at various potentials (Fig. 3 and *SI Appendix*, Fig. S19) in 0.1 M $KHCO_3$. The onset of C_2–C_3 formation was observed at only −0.57 V vs. RHE, with products mainly comprising C_2H_4, EtOH, and *n*-PrOH. Compared with that of the pristine copper foil (18), overpotentials were lowered by 180 mV for C_2H_4 and 390 mV for EtOH and *n*-PrOH, respectively (*SI Appendix*, Table S3). Beyond this potential, a substantial rise in C_2–C_3 FE was observed (*SI Appendix*, Table S4), with the highest selectivity toward C_2–C_3 products (55%) achieved at −0.86 V vs. RHE. The high selectivity for C_2–C_3 products, including oxygenates, is quite significant, compared with previously reported catalysts for C_2–C_3 product formation around similar overpotentials applied in neutral pH aqueous media (*SI Appendix*, Table S5). So far, catalysts for multicarbon products have been Cu-based (mostly derived from oxides or halides) and require bias applied close to and beyond −1 V vs. RHE (*SI Appendix*, Table S6), where even only some of them reach product distributions dominated by C_2–C_3 products (C_2–C_3 > C_1 + H_2). Furthermore, with major efforts in the field toward using oxidized Cu as a starting template, the discovery of this catalyst presents an approach to achieving high

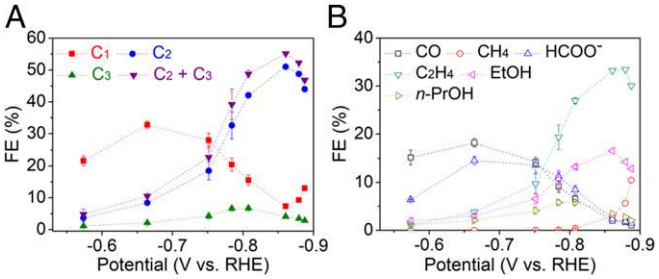

Fig. 3. Electrochemical CO_2 reduction activity of trans-CuEn. (*A*) FE of C_1, C_2, and C_3 products at various potentials for trans-CuEn. (*B*) FE of major products at various potentials for trans-CuEn. Electrochemical tests were conducted using 0.1 M $KHCO_3$ solution at 1 atm CO_2. Error bars shown are 1 SD from three independent measurements.

C_2–C_3 selectivity for electrochemical CO_2 reduction. In contrast, FE for two-electron reduced products (CO and formate) could be lowered to ~1%, implying that almost all of the CO_2 interacting with the catalyst could undergo C–C coupling to yield more complex products (Fig. 3*B*). In assessing catalytic performance for multicarbon product formation, earlier reports have been using C_2H_4/CH_4 FE ratio as a figure of merit and trans-CuEn exhibits significantly high values at low overpotentials (~252 at −0.78 V vs. RHE) that are comparable or better than previous catalysts reported for selective formation of C_2H_4 (*SI Appendix*, Fig. S20 and Table S7). More negative bias applied leads to increase in CH_4 formation and C_1 FE.

It has been suggested that larger cations promote higher concentrations of CO_2 near the catalyst surface, leading to increased activity (17, 47). For further optimization, Cu NP ensembles were tested in 0.1 M $CsHCO_3$ aqueous electrolyte saturated with 1 atm CO_2 and a similar trend was observed where increased loading densities resulted in higher C_2–C_3 selectivity (*SI Appendix*, Fig. S21). Transformation of Cu NP ensembles (at optimized condition of ×32.5 loading in 0.1 M $CsHCO_3$) consistently resulted in cube-shaped particles mixed together with smaller NPs (*SI Appendix*, Fig. S22), hereafter referred to as trans-CuEn 2. Activity of trans-CuEn 2 was measured at various potentials (Fig. 4 and *SI Appendix*, Fig. S23) and high C_2–C_3 selectivity was observed at more positive potentials with the onset of C_2–C_3 formation at only −0.53 V vs. RHE (*SI Appendix*, Table S3), which is 40 mV less of applied overpotential compared with that observed in 0.1 M $KHCO_3$. Highest C_2–C_3 selectivity (~50%) was observed at −0.75 V vs. RHE, shifting the potential 110 mV more positive relative to the point of maximum C_2–C_3 FE in 0.1 M $KHCO_3$. Therefore, with this catalytic structure, selective electrocatalytic conversion CO_2 to C_2–C_3 hydrocarbons and oxygenates could be achieved at significantly reduced overpotentials, compared with what have been demonstrated up to now (*SI Appendix*, Tables S5 and S6). Similarly, the main products were C_2H_4, EtOH, and *n*-PrOH (Fig. 4*B* and *SI Appendix*, Table S8) constituting up to 95% of total C_2–C_3 products (*SI Appendix*, Fig. S24). In addition, not only were FEs of CO and formate decreased to very low levels (1~2%), but CH_4 formation could also be suppressed (<1%) across the entire potential region, resulting in a significantly high C_2H_4/CH_4 ratio (~2,133 at −0.73 V vs. RHE) at low overpotentials (*SI Appendix*, Fig. S24 and Table S7). Owing to its high C_2–C_3 selectivity in 0.1 M $CsHCO_3$, the proportion of C_2–C_3 products among the total CO_2 reduced products reached up to 90% (Fig. 4*C*).

With the real surface area of trans-CuEn 2 measured (*SI Appendix*, Fig. S25), specific current density plots and Tafel slopes of the three major products could be obtained (Fig. 4*D*). Both C_2H_4 and EtOH exhibit similar slopes (~120 mV/dec), indicative of a rate-determining step with a common intermediate. Furthermore,

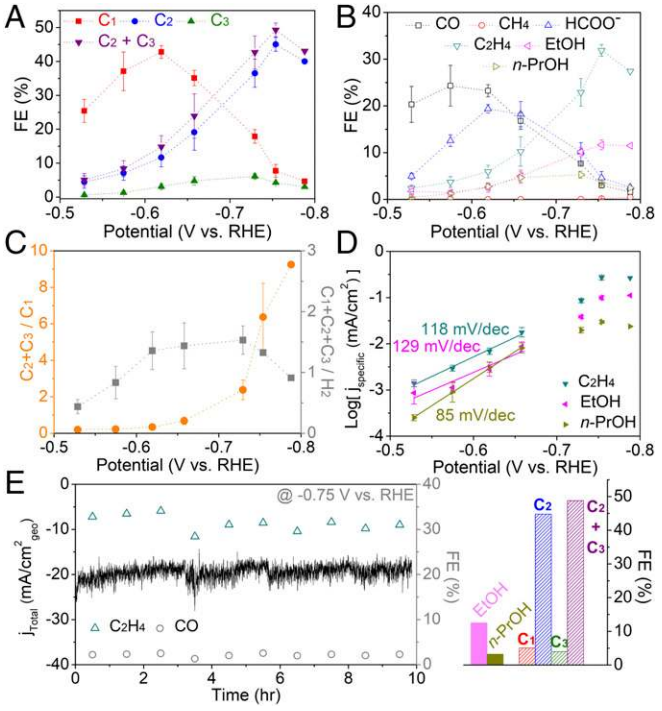

Fig. 4. Electrocatalytic behavior of trans-CuEn 2 (×32.5 loading in 0.1 M $CsHCO_3$). (*A*) FE of C_1, C_2, and C_3 products at various potentials. (*B*) FE of major products at various potentials. (*C*) Relative ratio of the FE. (*D*) Logarithmic specific current density (corrected by the real surface area of the catalyst) plots for C_2H_4, EtOH, and *n*-PrOH. Electrochemical tests were conducted in 0.1 M $CsHCO_3$ solution at 1 atm CO_2. Error bars shown are 1 SD from three independent measurements. (*E*) Long-term electrolysis at −0.75 V vs. RHE with gas products measured every hour. Column graph on the right shows FE of EtOH and *n*-PrOH measured after electrolysis and C_1, C_2, and C_3 product FEs for the overall run.

C_2H_4 and EtOH start forming in the potential region where CO evolution is dominant and increase while CO diminishes (Figs. 3*B* and 4*B*), suggesting that formation of these C_2 products is essentially limited by the coupling of major C_1 intermediates. It has been also shown that higher coverages of *CO can be expected in the region where CO formation is majorly observed (48). Therefore, with a slope close to 120 mV/dec suggesting a single electron transfer step, we expect the rate-determining step to be a reductive coupling (i.e., dimerization) step of adsorbed CO intermediates, predicted from theory and carbon monoxide reduction experiments on copper (43, 49–51):

$$*CO + *CO + e^- \rightarrow *C_2O_2^-.$$

On the other hand, *n*-PrOH exhibits a different slope, suggesting a distinct rate-determining step from that of C_2 products. Estimated value is rather close to that observed for CH_4 on copper foil (86 mV/dec) (38). In addition, it has been reported that *n*-PrOH formation only occurs when reactants include both CO (carbon monoxide) and C_2H_4, while CO reduction solely leads to EtOH (28). If C_3 products followed the same pathway as C_2 products, *n*-PrOH should have been observed upon CO reduction. Instead, it may be that *n*-PrOH formation requires coupling between CO and hydrogenated carbon [e.g., carbene ($*CH_2$)], which is a major intermediate in the pathway to CH_4 (50). CH_4 formation activity of trans-CuEn and -CuEn 2 supports this idea as well (Figs. 3*B* and 4*B* and *SI Appendix*, Tables S4 and S8). In contrast to C_2H_4 and EtOH, *n*-PrOH reaches peak selectivity at a more positive potential and the potential in which *n*-PrOH FE drops coincides well with the point where CH_4 FE starts to rise. However, it is still unclear how formation of C_3 products occur and an in-depth study of the mechanistic pathways to these products is needed.

Long-term stability was demonstrated by 10 h electrolysis of trans-CuEn 2 at −0.75 V vs. RHE (Fig. 4*E*). Average C_2–C_3 FE reached ∼50% for the overall run and structural features of trans-CuEn 2 were maintained as well (*SI Appendix*, Fig. S26). Furthermore, stable C_2–C_3 product current density of 10 mA/cm^2_{geo} was achieved, which is potentially attractive for solar-to-fuel applications. As long-term electrolysis accumulates significant amounts of liquid products, propionaldehyde, likely to be the precursor to *n*-PrOH, was detected (*SI Appendix*, Fig. S27).

Stable and selective C_2–C_3 product generation achieved by the structurally transformed Cu NP ensembles presents a promising future direction to renewables-powered artificial carbon cycle. Projected solar-to-fuel efficiencies of multicarbon products (*SI Appendix*, Fig. S28), assuming combination of commercial Si photovoltaic devices and electrolysis configurations recently demonstrated for effective syngas formation (52, 53), are comparable or better than natural photosynthesis (e.g., 2.8% for C_2H_4). Significant mass activities are achieved as well (*SI Appendix*, Fig. S29), desirable in terms of cost-effectiveness, due to extremely low mass (g_{Cu}) used compared with other methods that rely on bulk Cu oxidation.

Conclusions

We have shown how an ensemble of Cu NPs can enable selective electrocatalytic conversion of CO_2 to C_2–C_3 hydrocarbons and oxygenates at significantly reduced overpotentials. Structural evolution of densely arranged Cu NPs resulted in C_2–C_3 active nanostructures and experimental investigation of the parameters affecting structural transformation and their catalytic behavior was performed. With the discovery of this active catalytic structure formed in situ, efforts in deepening the understanding of how NPs and atoms within evolve under electrically biased and chemically relevant conditions seem necessary, which will shed light on the key structural features for CO_2 conversion to multicarbon products. Furthermore, we anticipate that the unique approach of using NPs as precursors to an active nanostructured material will lead to a wide expansion of the materials library for various catalytic applications.

Methods

Copper NPs in this work are synthesized by reducing copper precursors at high temperatures with tetradecylphosphonic acid used as surface ligands. Densely packed arrangement of copper NPs on carbon support is achieved by directly loading these particles in solution to a carbon-paper electrode. Copper NPs deposited electrodes are tested for electrochemical reduction of carbon dioxide in neutral pH aqueous environments (0.1 M $KHCO_3$ or $CsHCO_3$ at 1 atm CO_2), with products measured by gas chromatography and NMR. Original copper NPs and the structures formed during electrolysis are characterized by various methods, including electron microscopy, X-ray photoelectron spectroscopy, and cyclic voltammetry. Further details of the experimental methods are provided in *SI Appendix*.

ACKNOWLEDGMENTS. This work was supported by Director, Office of Science, Office of Basic Energy Sciences, Chemical Sciences, Geosciences, & Biosciences Division, of the US Department of Energy under Contract DE-AC02-05CH11231, FWP CH030201 (Catalysis Research Program). Transmission electron microscopy, scanning electron microscopy, and X-ray photoelectron spectroscopy were conducted using facilities at the National Center for Electron Microscopy and Imaging and Nanofabrication facilities at the Molecular Foundry. Work at the Molecular Foundry was supported by the Office of Science, Office of Basic Energy Sciences, of the US Department of Energy under Contract DE-AC02-05CH11231. This work made use of the facilities at the NMR Facility, College of Chemistry, University of California, Berkeley. Inductively coupled plasma atomic emission spectroscopy was supported by the Microanalytical Facility, College of Chemistry, University of California, Berkeley. D.K. acknowledges the support of Samsung Scholarship. C.S.K. acknowledges support by the Alexander von Humboldt Foundation.

1. EIA (2016) *International Energy Outlook 2016* (US Energy Information Administration, Washington, DC).
2. Lewis NS (2016) Research opportunities to advance solar energy utilization. *Science* 351:aad1920.
3. Liu C, Colón BC, Ziesack M, Silver PA, Nocera DG (2016) Water splitting-biosynthetic system with CO_2 reduction efficiencies exceeding photosynthesis. *Science* 352: 1210–1213.
4. Luo J, et al. (2014) Water photolysis at 12.3% efficiency via perovskite photovoltaics and Earth-abundant catalysts. *Science* 345:1593–1596.
5. Kim D, Sakimoto KK, Hong D, Yang P (2015) Artificial photosynthesis for sustainable fuel and chemical production. *Angew Chem Int Ed Engl* 54:3259–3266.
6. Vesborg PCK, Seger B, Chorkendorff I (2015) Recent development in hydrogen evolution reaction catalysts and their practical implementation. *J Phys Chem Lett* 6: 951–957.
7. Luc W, et al. (2017) Ag-Sn bimetallic catalyst with a core-shell structure for CO_2 reduction. *J Am Chem Soc* 139:1885–1893.
8. Wang Z, Yang G, Zhang Z, Jin M, Yin Y (2016) Selectivity on etching: Creation of high-energy facets on copper nanocrystals for CO_2 electrochemical reduction. *ACS Nano* 10:4559–4564.
9. Weng Z, et al. (2016) Electrochemical CO_2 reduction to hydrocarbons on a heterogeneous molecular Cu catalyst in aqueous solution. *J Am Chem Soc* 138:8076–8079.
10. Hall AS, Yoon Y, Wuttig A, Surendranath Y (2015) Mesostructure-induced selectivity in CO_2 reduction catalysis. *J Am Chem Soc* 137:14834–14837.
11. Asadi M, et al. (2016) Nanostructured transition metal dichalcogenide electrocatalysts for CO_2 reduction in ionic liquid. *Science* 353:467–470.
12. Zhu W, et al. (2014) Active and selective conversion of CO_2 to CO on ultrathin Au nanowires. *J Am Chem Soc* 136:16132–16135.
13. Chen Y, Li CW, Kanan MW (2012) Aqueous CO_2 reduction at very low overpotential on oxide-derived Au nanoparticles. *J Am Chem Soc* 134:19969–19972.
14. Gao S, et al. (2016) Partially oxidized atomic cobalt layers for carbon dioxide electroreduction to liquid fuel. *Nature* 529:68–71.
15. Liu M, et al. (2016) Enhanced electrocatalytic CO_2 reduction via field-induced reagent concentration. *Nature* 537:382–386.
16. Kim D, Resasco J, Yu Y, Asiri AM, Yang P (2014) Synergistic geometric and electronic effects for electrochemical reduction of carbon dioxide using gold-copper bimetallic nanoparticles. *Nat Commun* 5:4948.
17. Hori Y (2008) Electrochemical CO2 reduction on metal electrodes. *Modern Aspects of Electrochemistry* (Springer, New York), pp 89–189.
18. Kuhl KP, Cave ER, Abram DN, Jaramillo TF (2012) New insights into the electrochemical reduction of carbon dioxide on metallic copper surfaces. *Energy Environ Sci* 5:7050.
19. Kas R, et al. (2014) Electrochemical CO_2 reduction on Cu_2O-derived copper nanoparticles: Controlling the catalytic selectivity of hydrocarbons. *Phys Chem Chem Phys* 16:12194–12201.
20. Chen CS, Wan JH, Yeo BS (2015) Electrochemical reduction of carbon dioxide to ethane using nanostructured Cu_2O-derived copper catalyst and palladium(II) chloride. *J Phys Chem C* 119:26875–26882.
21. Kim D, et al. (2015) Insights into an autonomously formed oxygen-evacuated Cu_2O electrode for the selective production of C_2H_4 from CO_2. *Phys Chem Chem Phys* 17: 824–830.
22. Chen CS, et al. (2015) Stable and selective electrochemical reduction of carbon dioxide to ethylene on copper mesocrystals. *Catal Sci Technol* 5:161–168.
23. Lee S, Kim D, Lee J (2015) Electrocatalytic production of C3-C4 compounds by conversion of CO_2 on a chloride-induced bi-phasic Cu_2O-Cu catalyst. *Angew Chem Int Ed Engl* 54:14701–14705.
24. Dutta A, Rahaman M, Luedi NC, Mohos M, Broekmann P (2016) Morphology matters: Tuning the product distribution of CO_2 electroreduction on oxide-derived Cu foam catalysts. *ACS Catal* 6:3804–3814.
25. Kwon Y, Lum Y, Clark EL, Ager JW, Bell AT (2016) CO_2 electroreduction with enhanced ethylene and ethanol selectivity by nanostructuring polycrystalline copper. *ChemElectroChem* 3:1012–1019.
26. Loiudice A, et al. (2016) Tailoring copper nanocrystals towards C_2 products in electrochemical CO_2 reduction. *Angew Chem Int Ed Engl* 55:5789–5792.
27. Ren D, et al. (2015) Selective electrochemical reduction of carbon dioxide to ethylene and ethanol on copper(I) oxide catalysts. *ACS Catal* 5:2814–2821.
28. Ren D, Wong NT, Handoko AD, Huang Y, Yeo BS (2016) Mechanistic insights into the enhanced activity and stability of agglomerated Cu nanocrystals for the electrochemical reduction of carbon dioxide to n-propanol. *J Phys Chem Lett* 7:20–24.
29. Mistry H, et al. (2016) Highly selective plasma-activated copper catalysts for carbon dioxide reduction to ethylene. *Nat Commun* 7:12123.
30. Handoko AD, et al. (2016) Mechanistic insights into the selective electroreduction of carbon dioxide to ethylene on Cu_2O-derived copper catalysts. *J Phys Chem C* 120: 20058–20067.
31. Song Y, et al. (2016) High-selectivity electrochemical conversion of CO_2 to ethanol using a copper nanoparticle/N-doped graphene electrode. *ChemistrySelect* 1:6055–6061.
32. Roberts FS, Kuhl KP, Nilsson A (2015) High selectivity for ethylene from carbon dioxide reduction over copper nanocube electrocatalysts. *Angew Chem Int Ed Engl* 54:5179–5182.
33. Ren D, Ang BS-H, Yeo BS (2016) Tuning the selectivity of carbon dioxide electroreduction toward ethanol on oxide-derived Cu_xZn catalysts. *ACS Catal* 6:8239–8247.
34. Gao D, et al. (2017) Plasma-activated copper nanocube catalysts for efficient carbon dioxide electroreduction to hydrocarbons and alcohols. *ACS Nano* 11:4825–4831.
35. Hori Y, Takahashi I, Koga O, Hoshi N (2003) Electrochemical reduction of carbon dioxide at various series of copper single crystal electrodes. *J Mol Catal Chem* 199:39–47.
36. Li CW, Ciston J, Kanan MW (2014) Electroreduction of carbon monoxide to liquid fuel on oxide-derived nanocrystalline copper. *Nature* 508:504–507.
37. Hoang TTH, Ma S, Gold JI, Kenis PJA, Gewirth AA (2017) Nanoporous copper films by additive-controlled electrodeposition: CO_2 reduction catalysis. *ACS Catal* 7:3313–3321.
38. Manthiram K, Beberwyck BJ, Alivisatos AP (2014) Enhanced electrochemical methanation of carbon dioxide with a dispersible nanoscale copper catalyst. *J Am Chem Soc* 136:13319–13325.
39. Kim Y-G, Javier A, Baricuatro JH, Soriaga MP (2016) Regulating the product distribution of CO reduction by the atomic-level structural modification of the Cu electrode surface. *Electrocatalysis* 7:391–399.
40. Kim Y-G, et al. (2016) Surface reconstruction of pure-Cu single-crystal electrodes under CO-reduction potentials in alkaline solutions: A study by seriatim ECSTM-DEMS. *J Electroanal Chem* 780:290–295.
41. Eilert A, et al. (2017) Subsurface oxygen in oxide-derived copper electrocatalysts for carbon dioxide reduction. *J Phys Chem Lett* 8:285–290.
42. Mistry H, et al. (2016) Tuning catalytic selectivity at the mesoscale via interparticle interactions. *ACS Catal* 6:1075–1080.
43. Varela AS, Kroschel M, Reier T, Strasser P (2016) Controlling the selectivity of CO_2 electroreduction on copper: The effect of the electrolyte concentration and the importance of the local pH. *Catal Today* 260:8–13.
44. Kas R, Kortlever R, Yılmaz H, Koper MTM, Mul G (2015) Manipulating the hydrocarbon selectivity of copper nanoparticles in CO_2 electroreduction by process conditions. *ChemElectroChem* 2:354–358.
45. Ma S, et al. (2016) One-step electrosynthesis of ethylene and ethanol from CO_2 in an alkaline electrolyzer. *J Power Sources* 301:219–228.
46. Wu J, et al. (2016) A metal-free electrocatalyst for carbon dioxide reduction to multicarbon hydrocarbons and oxygenates. *Nat Commun* 7:13869.
47. Singh MR, Kwon Y, Lum Y, Ager JW, 3rd, Bell AT (2016) Hydrolysis of electrolyte cations enhances the electrochemical reduction of CO_2 over Ag and Cu. *J Am Chem Soc* 138:13006–13012.
48. Huang Y, Handoko AD, Hirunsit P, Yeo BS (2017) Electrochemical reduction of CO_2 using copper single-crystal surfaces: Effects of CO* coverage on the selective formation of ethylene. *ACS Catal* 7:1749–1756.
49. Calle-Vallejo F, Koper MTM (2013) Theoretical considerations on the electroreduction of CO to C2 species on Cu(100) electrodes. *Angew Chem Int Ed Engl* 52:7282–7285.
50. Kortlever R, Shen J, Schouten KJP, Calle-Vallejo F, Koper MTM (2015) Catalysts and reaction pathways for the electrochemical reduction of carbon dioxide. *J Phys Chem Lett* 6:4073–4082.
51. Pérez-Gallent E, Figueiredo MC, Calle-Vallejo F, Koper MTM (2017) Spectroscopic observation of a hydrogenated CO dimer intermediate during CO reduction on Cu (100) electrodes. *Angew Chem Int Ed Engl* 56:3621–3624.
52. Vermaas DA, Smith WA (2016) Synergistic electrochemical CO_2 reduction and water oxidation with a bipolar membrane. *ACS Energy Lett* 1:1143–1148.
53. Li YC, et al. (2016) Electrolysis of CO_2 to syngas in bipolar membrane-based electrochemical cells. *ACS Energy Lett* 1:1149–1153.